


Fast nuclear-spin entangling gates compatible with large-scale atomic arrays

Xiao-Feng Shi  and Yan Lu 

Center for Theoretical Physics and School of Physics and Optoelectronic Engineering, Hainan University, Haikou 570228, China and School of Physics, Xidian University, Xi'an 710071, China

 (Received 30 November 2023; revised 16 February 2024; accepted 14 May 2024; published 12 July 2024)

Fast nuclear-spin entangling gates of divalent atoms can be realized with one global laser pulse when $\Delta_Z < \Omega$, where Δ_Z is the Zeeman-splitting-dominated frequency difference between the two clock-Rydberg transitions of the two qubit states and Ω is the maximal Rabi frequency. The condition $\Delta_Z < \Omega$ and the sensitivity of Rydberg-state energy to magnetic fluctuation demand the magnetic field to be weak, making the gate compatible with large-scale atomic arrays because weaker magnetic fields can be smoother in a large qubit array. The gate can have a high fidelity for the decoherence of Rydberg states, which limits the gate fidelity and grows with $1/\Omega$, can be mitigated with easily attainable large Ω .

DOI: [10.1103/PhysRevA.110.012610](https://doi.org/10.1103/PhysRevA.110.012610)

I. INTRODUCTION

Quantum computing requires both scalability and accuracy [1–3], for which several physical platforms have exhibited high controllability on the single quantum level over several tens of qubits [4–6], yet it remains prohibitive to realize both a large-scale qubit array and universal quantum logic gates executable with qubits in any location of a large array.

It was recently demonstrated that hundreds of individual neutral atoms can be assembled to a single quantum memory [7–9], but scaling a neutral-atom qubit array without hampering its controllability is not straightforward though atom arrays with over 1000 atoms [9], high-fidelity single-qubit [10–13] and two-qubit [5,14,15] gates, and small-scale quantum processors [16–18] were already demonstrated with neutral atoms. The headache partly arises from two issues. First, for an alkali-metal atomic qubit array as in [5,16,17,19–32], the spatial change of magnetic field Bz in an anticipated large-scale array with practically useful millions of qubits [33] can result in spatial variation of the qubit frequency, which inevitably makes the qubits no longer identical. See Appendix A for the details on the qubit frequency in the presence of magnetic field variation in a large atomic array. Second, the error in a Rydberg-mediated entangling gate [5,16,17,19–29,31,32] is dominated by the dephasing of the ground-Rydberg transition, radiative decay of the Rydberg state, atomic position fluctuation, and scattering at the intermediate state (in the case of two-photon Rydberg excitation) [5,28], all growing with the increase of the duration of the Rydberg excitation pulse. Effective suppression of these errors can be achieved by using large Rydberg Rabi frequency Ω . For alkali-metal atoms, unfortunately, unless a one-photon ultraviolet Rydberg excitation is employed [23,30], an intermediate state is often needed [5,16,17,19–22,24–29,31,32] at which the scattering strongly limits Ω [5].

One solution to the above issues is encoding qubits by nuclear spins in the clock state of alkaline-earth-like atoms. Even in the presence of spin-orbit and hyperfine

interaction induced state mixing [34], the clock state still has a g factor of the nuclear-spin character which renders a sensitivity to the magnetic field that is three orders of magnitude weaker than that of a hyperfine qubit, making nuclear-spin qubits more compatible with large-scale atom arrays. Moreover, one-photon Rydberg excitation of the clock state of an alkaline-earth-like atom with $\Omega > 2\pi \times 10$ MHz is much easier [35] compared to that of an alkali-metal atom [36], and thereby can potentially enhance the gate fidelity since the intermediate state scattering is absent and Rydberg-state decay can be suppressed with much shorter gate duration. However, using entangling protocols designed for alkali-metal atoms [27,37,38] with nuclear-spin qubits requires $\Delta_Z \gg \Omega$ (e.g., the Rydberg excitation in the nuclear-spin gates of [15,39] had Δ_Z/Ω equal to 5.8 and 10.6, respectively), where Δ_Z is the Zeeman-splitting-dominated detuning for the Rydberg excitation of the two nuclear-spin qubit states. Gates in the condition $\Delta_Z \gg \Omega$ will be slow under a Gauss-scale B field, or magnetic noise can be significant if strong B fields are used for speeding up the gate. It is a demanding task to find a fast gate with $\Delta_Z/\Omega < 1$ when, meanwhile, the gate can be conveniently executed by only one global laser pulse [5,15].

Here, with the qubit encoded in the clock state of an alkaline-earth-like atom so that large Ω is realizable [35], we study entangling gates realized under the condition $\Delta_Z/\Omega < 1$ via one ultraviolet laser pulse. The short gate duration and the absence of intermediate-state scattering can help to yield readily attainable high-fidelity gates for Ω over $2\pi \times 10$ MHz [35]. Importantly, a Gauss-scale B field can be used without compromising the gate speed, and thus the gate is compatible with a large atomic array because, in order to have approximately the same B field throughout the whole atomic array, the array must be placed, e.g., near the center of an exceedingly large solenoid where the large size decreases the B field.

The remainder of this article is organized as follows. In Sec. II, we briefly introduce the gate. In Sec. III, we study how fast the gate can be with a linearly polarized field when there is a limit on the B field in a large-scale atom array. In Sec. IV, we

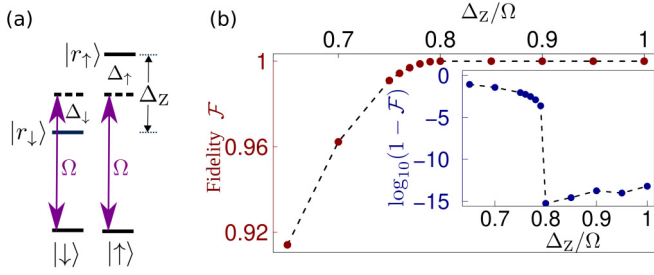


FIG. 1. (a) A π -polarized ultraviolet laser sent to, as an example, a ^{171}Yb atom, exciting two nuclear-spin qubit states $|\uparrow\rangle \equiv |(6s^2)^3P_0 |I = 1/2, m_I = 1/2\rangle$ and $|\downarrow\rangle \equiv |(6s^2)^3P_0 |I = 1/2, m_I = -1/2\rangle$ to the Rydberg states $|r_\uparrow\rangle, |r_\downarrow\rangle \equiv (6s6p)^3S_1 |F = 3/2, m_F = \pm 1/2\rangle$ with a Rabi frequency Ω . (b) By assuming perfect blockade and with a pulse duration $3\pi/\Omega$, a CZ-like gate in Eq. (1) can be realized by smoothly changing the phase of the laser. Shown is the gate fidelity \mathcal{F} and the common logarithm of the infidelity in the inset with a corresponding optimized pulse for each Δ_Z/Ω .

consider the gate fidelity when the laser field is not perfectly polarized as desired. In Sec. V, we study the gate by using circular laser fields and its robustness against polarization impurity in the laser field. In Sec. VI, we show that the gate is applicable when Rydberg interactions are both finite and fluctuating. Section VII gives a discussion and a conclusion. Details of the impact of magnetic fluctuation, the method of numerical optimization, and Hamiltonians are grouped in the Appendixes.

II. A CZ-LIKE QUANTUM GATE

The CZ-like quantum logic gate in this article is realized by phase accumulation of two-qubit nuclear-spin states in detuned Rydberg excitation [27,37,40] under the blockade condition [41,42]. With qubits encoded in two nuclear-spin Zeeman substates of the clock state of an alkaline-earth-like atom such as ^{171}Yb [15], $|\uparrow(\downarrow)\rangle \equiv (6s6p)^3P_0 |m_I = \pm 1/2\rangle$, the gate maps the four computational basis states as

$$\begin{aligned} |\uparrow\uparrow\rangle &\mapsto e^{i\alpha}|\uparrow\uparrow\rangle, \\ |\uparrow\downarrow\rangle &\mapsto e^{i(\alpha+\beta)/2}|\uparrow\downarrow\rangle, \\ |\downarrow\uparrow\rangle &\mapsto e^{i(\alpha+\beta)/2}|\downarrow\uparrow\rangle, \\ |\downarrow\downarrow\rangle &\mapsto -e^{i\beta}|\downarrow\downarrow\rangle, \end{aligned} \quad (1)$$

which can be transformed to the canonical controlled-Z (CZ) gate by single-qubit gates $\{|\uparrow\rangle, |\downarrow\rangle\} \mapsto \{e^{-i\alpha/2}|\uparrow\rangle, e^{-i\beta/2}|\downarrow\rangle\}$. The two-qubit states in each atom are nearly degenerate in a Gauss-scale magnetic field $B\mathbf{z}$, and during the excitation to two hyperfine-Zeeman substates $|r_{\uparrow,\downarrow}\rangle$ of a $(6s6p)^3S_1$ Rydberg state with one laser field [43–46], the two nuclear-spin states have a detuning difference $\Delta_Z \equiv |\Delta_\uparrow - \Delta_\downarrow|$ which is approximately the Zeeman splitting $\Delta_Z \approx 2\pi \times 1.9B$ MHz/G [45] between $|r_\uparrow\rangle$ and $|r_\downarrow\rangle$ [15,39,43–46], where $\Delta_{\uparrow,\downarrow}$ is the detuning of the laser field with respect to $|r_{\uparrow,\downarrow}\rangle$ shown in Fig. 1(a). During the clock-Rydberg excitation, when $\Delta_{\uparrow,\downarrow}$ is comparable to the Rabi frequency Ω , a significant phase can arise when both $\Delta_{\uparrow,\downarrow}$ and Ω are fixed [40,46]. But this makes a simultaneous restoration of the four computational basis states back to themselves impossible unless

TABLE I. N (second row) indicates the minimal gate duration $2\pi N/\Omega$ required to realize a CZ-like gate in Eq. (1) as a function of Δ_Z/Ω when the infidelity [47] can be smaller than 10^{-7} when assuming infinite Rydberg blockade interaction in the numerical optimization [48,49] and absence of Rydberg-state decay; details for the numerical optimization method can be found in Appendix B. Here, $\Delta_Z \equiv |\Delta_\uparrow - \Delta_\downarrow|$ and change of ratio between Δ_\uparrow and Δ_\downarrow do not alter the results here. Too small Δ_Z does not work. For example, $\Delta_Z/\Omega = 0.55$ leads to $\mathcal{F} \lesssim 0.991$ when $N \leq 1.9$, where we restrict the value of N because the condition $N > 1.9$ brings no advantage on the gate duration in units of $1/\Delta_Z$ compared to the cases here.

$\frac{\Delta_Z}{\Omega}$	0.6	0.65	0.7	0.75	0.8	0.85	0.9	0.95	1
N	1.843	1.733	1.646	1.568	1.497	1.434	1.376	1.325	1.291

multiple laser pulses are used [46], so we consider a smooth change of laser phase when only one global laser pulse is used [5,15,38]. A smooth change of laser frequency can also be used, but it can lead to more population leakage via undesired transitions due to the polarization impurity of the laser field. Therefore, we focus on a smooth change of laser phase and $\Delta_Z/2 = -\Delta_\uparrow = \Delta_\downarrow$ so that undesired transitions due to polarization impurity of laser fields are more detuned, as discussed later.

To study quantum gates compatible with large atom arrays, small B field and gate time are favorable, and meanwhile the gate fidelity must be large. In Secs. III–V, we assume that the dipole-dipole interaction V between the two atoms when both are in Rydberg states is infinite so that we can theoretically investigate how fast the gate can be under a certain B field or how small the B field can be when we fix the gate duration. This is because when we consider the blockade regime, V/Ω can be huge [33,50–58]; when we use a finite V in the numerical simulation, a dynamical phase can arise and its value is sensitive to V [46]; and when V is fixed, optimal control [38,59–70] can locate a V -dependent pulse for a high-fidelity gate, as shown in Sec. VI.

We show gate protocols either by a linearly polarized field or by a circularly polarized field. Below, we begin with a linearly polarized laser field which was often employed [15].

III. LIMIT OF GATE SPEED

To find a gate with a fast speed so as to have a high fidelity, and meanwhile be compatible with a large array, we note that the value of Ω for the clock-Rydberg transition can be quite large [35], but the CZ-like gate shall be executed with an Ω that has a certain ratio to Δ_Z as indicated in Table I, and therefore Δ_Z is the key parameter limiting the gate speed in the regime $\Delta_Z/\Omega < 1$. In order to have a high-fidelity gate with any atom pair in a large-scale atomic array by using one set of lasers, the B field or Δ_Z should be small. To understand this, consider the qubit array with 1305 atoms in a $\sim 0.2 \times 0.2$ mm area reported in Ref. [9]. For a practically useful quantum computer with, e.g., a million atoms [33], we would anticipate a scaling of the array in [9] to a larger one in a 6×6 mm area. If the coil to ensure a smooth magnetic field throughout the qubit array in Ref. [9] has a radius of 30 cm, then we would need another coil with a radius of 9 m for

the million-qubit atomic array to ensure a similarly smooth magnetic field. Though it sounds crazy, it is not a forbidden task and worthy concerning the benefits a practical quantum computer can bring to us [71–73]. But with such a large coil, it is, in general, not easy to generate a strong and stable B field at the qubit array, so we can assume B smaller than, say, 10 G [5,15,17,19–28,32,39], at which $\Delta_Z/2\pi = 19$ MHz in the case of ^{171}Yb . This assumption is made also because weaker B fields have a smaller fluctuation [74]. When we fix the gate duration with a given Ω , there is a minimal magnetic field below which the gate in Eq. (1) cannot be realized, as shown in Fig. 1(b). For example, with a gate duration of $3\pi/\Omega$, pulses can be found to yield a unit fidelity when $\Delta_Z/\Omega \gtrsim 0.8$. On the other hand, it is desirable to implement a gate within a short time, $2\pi N/\Omega$ [5,15,38]. We find that the smallest N is about 1.3 when Δ_Z/Ω is 1, and when Δ_Z/Ω decreases, N grows. Moreover, a too small Δ_Z is not suitable for a fast gate. With a decrease of 0.05 from $\Delta_Z/\Omega = 1$, Table I shows that the smallest Δ_Z/Ω is 0.6 for realizing a gate in Eq. (1), with a gate duration of about $2.21\pi/\Delta_Z$, which is about 58 ns when $B = 10$ G. In experiments, the laser field can have rise and fall edges. With the rise and fall edges included, one can still realize the CZ-like gate, with one example shown in Fig. 2. The phase profile in Fig. 2(a) is slightly different from the corresponding one without rise and fall edges. The example of Fig. 2 has a Rydberg superposition time $2\pi/\Omega$, leading to a Rydberg-state decay error of $1.6\pi/(\tau\Delta_Z)$, which is about 4.2×10^{-4} with $B = 10$ G if $\tau = 100 \mu\text{s}$ [46], so the decay-induced error is greatly suppressed. Besides the suppression of the Rydberg-state decay, the fast speed suppresses the error from the motion-induced dephasing, too. For example, in a recent experiment [5], a high-fidelity entangling gate was realized with a gate duration of less than 260 ns.

IV. POLARIZATION IMPURITY OF LASER FIELDS

The laser field can have impure polarization, leading to unwanted transitions, as in Fig. 2, so that the gate map in Eq. (1) becomes a 4×4 matrix where the relevant [75] diagonal elements give the gate map $\text{diag}\{ae^{i\alpha}, be^{i(\alpha+\beta)/2}, be^{i(\alpha+\beta)/2}, -ce^{i(\beta+\epsilon)}\}$, with $a, b, c < 1$ and ϵ a residual phase. The gate map becomes $\mathcal{U} = \text{diag}\{a, b, b, -ce^{i\epsilon}\}$ with single-qubit gates, where the difference from the ideal gate $U = \text{diag}\{1, 1, 1, -1\}$ derived from Eq. (1) by single-qubit gates can be characterized by the fidelity [47]

$$\mathcal{F} = [|\text{Tr}(\hat{U}^\dagger \hat{U})|^2 + \text{Tr}(\hat{U}^\dagger \hat{U} \hat{U}^\dagger \hat{U})]/20. \quad (2)$$

We consider the power ratio between the π , σ^+ , and σ^- polarized fields as $1 : \zeta_0\zeta/(1+\zeta) : \zeta_0/(1+\zeta)$, where ζ_0 is the intensity ratio of the wrong field to the desired field, and characterize the rates for the undesired transitions denoted by the dashed and dotted arrows in Fig. 3 with angular momentum selection rules [76], based on which we have simulated the gate fidelity shown in Fig. 4. Two features appear in Fig. 4. First, \mathcal{F} is still large in the presence of polarization impurity, and $\mathcal{F} > 0.999$ when $\zeta_0 < 0.0004$. So, the gate can attain a high fidelity in practical implementation, for the intensity ratio of the wrong field to the desired field can be as small as 10^{-4} , as in the experiment of Ref. [77]. Second, the fidelity

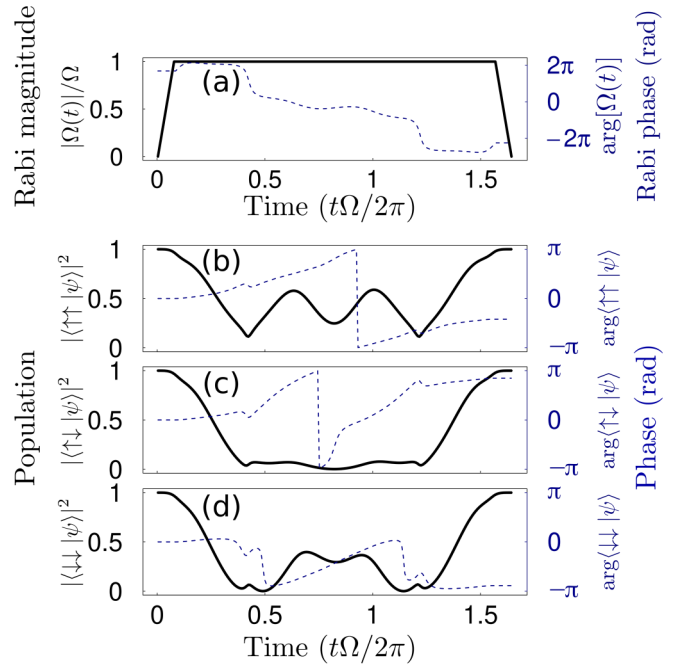


FIG. 2. State dynamics for the CZ-like gate by π -polarized laser field with $\frac{\Delta_Z}{\Omega} = 0.8$, $\Delta_\downarrow = -\Delta_\uparrow = \Delta_Z/2$. (a) The amplitude and phase of $\Omega(t)$. (b)–(d) The population (solid curve) and phase (dashed curve) of the ground-state component of the wave function when the input states are $|\uparrow\uparrow\rangle$, $|\uparrow\downarrow\rangle$, and $|\downarrow\downarrow\rangle$, respectively; the state dynamics for $|\downarrow\uparrow\rangle$ is similar to that of $|\uparrow\downarrow\rangle$. Rydberg-state decay and blockade leakage are ignored here. The Rydberg superposition time is about $2\pi/\Omega$ averaged over the four input states. Here the gate duration is 10% longer than $2\pi N/\Omega$ where $N = 1.497$, for we have added a rise and fall edge of $\Omega(t)$, each of duration $\pi N/(10\Omega)$; the counterpart to this figure without the rise and fall edges is shown in Appendix C. Since the simultaneous modulation of laser intensity and phase may be more challenging compared to the modulation of either intensity or phase, here the phase of the rise and fall edge is constant.

shows an unequal dependence on the ratios of the σ^+ and the σ^- polarized fields, and it appears that the error is smaller if the wrong polarization is mainly σ^+ . This is because, as shown in Figs. 2(b)–2(d), the final phase in the input state $|\uparrow\uparrow\rangle$ has a more pronounced value for determining the final π phase of the gate map. The σ^- transition can induce an undesired transition from $|\uparrow\rangle$ to $|r_\downarrow\rangle$, which does more harm to the dynamics of $|\uparrow\rangle$ compared to the σ^+ transition that induces an undesired transition from $|\uparrow\rangle$ to $|r_+\rangle$ because the detuning $\Delta_Z/2$ for $|\uparrow\rangle \rightarrow |r_\downarrow\rangle$ is three times smaller than the detuning $-3\Delta_Z/2$ for $|\uparrow\rangle \rightarrow |r_+\rangle$.

It is, in principle, feasible to suppress the gate errors from the polarization impurity of the laser fields. The impure polarization of a laser field is mainly from the misalignment of its propagation direction and the quantization axis that is usually specified by a magnetic field [77], both being fixed during the gate sequence. So the laser-polarization impurity can be determined [77–79]. Therefore, with a certain set of ζ_0 and ζ , it is, in principle, possible to find optimal pulses [38,59–70] for maximizing the gate fidelity. But even without doing so, Fig. 4 indicates that our gate protocol based on an easily

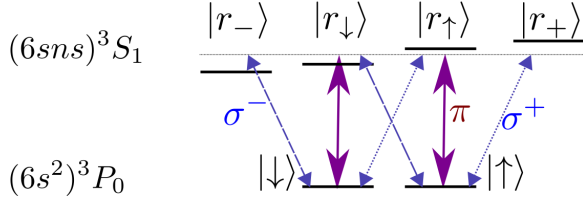


FIG. 3. Schematic of polarization impurity in the laser field for the gate realized with a π -polarized field. Thicker arrows indicate the desired transitions, while thinner arrows show transitions induced by unwanted σ^\pm -polarized laser fields. Fields of both the correct and wrong polarization have a common frequency so that they are tuned to a virtual level, denoted by the dashed line. The Zeeman splitting between $|\uparrow\rangle$ and $|\downarrow\rangle$ is negligible. The detunings are $\Delta_{\uparrow,\downarrow}$ at $|r_{\uparrow,\downarrow}\rangle$, and $\Delta_{\uparrow} - \Delta_Z$ and $\Delta_{\downarrow} + \Delta_Z$ at $|r_{\pm}\rangle$, respectively. The numerical results in this article are with $\Delta_{\downarrow} = -\Delta_{\uparrow} = \Delta_Z/2$ so that $|r_{\pm}\rangle$ are both more detuned to suppress the unwanted transitions.

attainable linearly polarized laser can yield high fidelity because ζ_0 can be made as small as 10^{-4} in the experiment of Ref. [77]. Given the fact that the polarization purity in [77] was achieved many years ago with circularly polarized fields, it is reasonable to assume that technology has been advancing and a higher purity is possible with the gate here since linear polarization is easier to prepare.

V. GATE WITH RIGHT-HAND POLARIZED LASER FIELD

We then study gates by a circularly polarized laser field. A circularly polarized field is more involved to prepare, but supposing that in the near future it will be possible to prepare a circularly polarized field with very high purity, it is worthy to consider whether there is any advantage to realize the gate with, e.g., σ^+ -polarized laser fields. By using a right-hand polarized field, the desired transitions for the two-qubit states are schematically shown in Fig. 5, where the difference between the magnitudes of the two Rabi frequencies arises from the

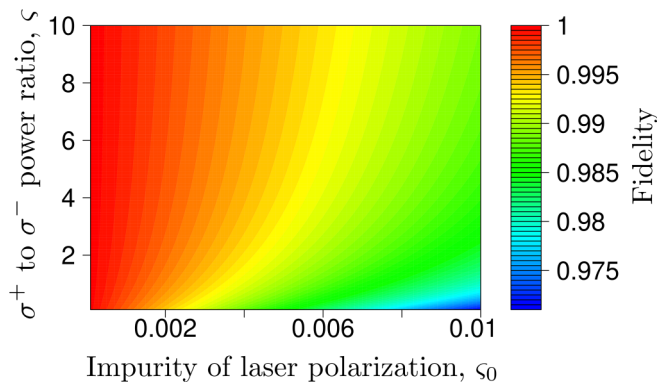


FIG. 4. Fidelity of the gate by linearly polarized laser fields with the pulse in Fig. 2(a) when there is polarization impurity in the laser characterized by the power ratio $\zeta_0 \in [10^{-4}, 10^{-2}]$ and $\zeta \in [0.1, 10]$, where ζ_0 is the intensity ratio of the wrong field to the desired field and ζ is the intensity ratio of the σ^+ to the σ^- polarized fields. Here, $\mathcal{F} > 0.999$ with $\zeta_0 < 4 \times 10^{-4}$, $\mathcal{F} > 0.99$ with $\zeta_0 < 3 \times 10^{-3}$, and the maximal and minimal \mathcal{F} are 0.9999 and 0.9712 with (ζ_0, ζ) equal to $(10^{-4}, 10)$ and $(0.01, 0.1)$, respectively.

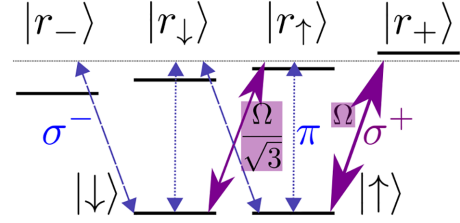


FIG. 5. A right-hand polarized ultraviolet laser exciting $|\uparrow\rangle \equiv |(6s^2)^3P_0 |I = 1/2, m_I = 1/2\rangle$ and $|\downarrow\rangle \equiv |(6s^2)^3P_0 |I = 1/2, m_I = -1/2\rangle$ to $|r_+\rangle \equiv (6sns)^3S_1 |F = 3/2, m_F = 3/2\rangle$, $|r_\uparrow\rangle \equiv (6sns)^3S_1 |F = 3/2, m_F = 1/2\rangle$ with a Rabi frequency Ω and $\Omega/\sqrt{3}$, respectively, where the arrow for the transition $|\uparrow\rangle \leftrightarrow |r_+\rangle$ being thicker compared to that for $|\downarrow\rangle \leftrightarrow |r_\uparrow\rangle$ indicates a difference of factor $\sqrt{3}$ in their Rabi frequencies due to angular momentum conservation. Dashed and dotted arrows indicate transitions by laser fields of wrong polarization.

angular momentum selection rule [76], as listed in Eq. (D1). Table II shows the approximate minimal gate duration $2\pi N/\Omega$ required to realize a CZ-like gate in Eq. (1) as a function of Δ_Z/Ω . Here, due to the long search time for each case, we did not use the step 0.001 for searching N as in Table I, but instead used 0.1. Another reason for this is that with a smaller step of 0.1, Table II shows that the minimal N does not decrease when Δ_Z/Ω grows as in Table I. This appears because the case in Sec. III and the case here are quite different in that the two nuclear-spin states are excited with equal Rabi frequencies in Sec. III. But here, the two nuclear-spin qubit states have different Rabi frequencies, as indicated in Fig. 5. Similar to Sec. III, we find that when we change the Δ_{\uparrow} to Δ_{\downarrow} ratio, the results on the gate speed in Table II stay the same.

As for the limit of gate speed under a certain magnetic field, Table II shows that the gate can be realized with $\Delta_Z/\Omega = 0.45$, where the gate duration is $1.8\pi/\Delta_Z$. But there is another case with $\Delta_Z/\Omega = 0.5$ where the gate duration is also $1.8\pi/\Delta_Z$, which is about 47 ns when $B = 10$ G. Such a fast speed is competitive with that in superconducting qubits, as reviewed in [58].

Laser fields can have impure polarization. So we examine the robustness to uncertainties in laser polarization when the gate is executed by a circularly polarized laser field. We label the power ratio between σ^+ , π , and σ^- polarized fields by $1 : \zeta_0\zeta/(1 + \zeta) : \zeta_0/(1 + \zeta)$, where ζ_0 is the intensity ratio of the wrong field to the desired field, and ζ is the ratio

TABLE II. Gate speed by using a right-hand polarized ultraviolet laser as in Fig. 5 when assuming infinite Rydberg blockade interaction in the numerical optimization [48,49] and absence of Rydberg-state decay. N (second row) indicates the approximately minimal gate duration $2\pi N/\Omega$ required to realize a CZ-like gate in Eq. (1) as a function of Δ_Z/Ω when the infidelity [47] can be smaller than 10^{-7} . Here, N is approximate because a step of 0.1 was taken in the numerical search for the minimal N , instead of 0.001 as in Table I.

$\frac{\Delta_Z}{\Omega}$	0.45	0.5	0.55	0.6	0.65	0.7	0.75	0.8	0.85	0.9	0.95	1
N	2.0	1.8	2.1	1.8	1.6	1.5	1.5	1.4	1.4	1.5	1.5	1.5

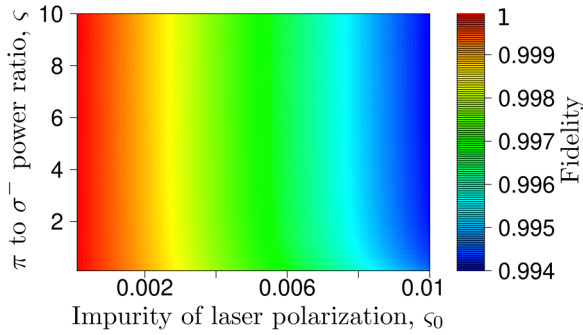


FIG. 6. Fidelity of the gate by σ^+ -polarized laser field with the pulse in Fig. 12(a) when there is polarization impurity in the laser characterized by $\xi_0 \in [10^{-4}, 10^{-2}]$ and $\xi \in [0.1, 10]$, where ξ_0 is the intensity ratio of the wrong field to the desired field and ξ is the intensity ratio of the π to the σ^- polarized fields. Here, $\mathcal{F} > 0.999$ with $\xi_0 < 1.7 \times 10^{-3}$ and $\mathcal{F} > 0.994$ for all data shown here. The maximal and minimal \mathcal{F} are at the lower-left and upper-right corners.

of the π to σ^- polarized fields. The rates for the undesired transitions denoted by the dashed and dotted arrows in Fig. 5 are given in Appendix D. With the optimized phase profile shown in Appendix D for a gate with $\Delta_Z/\Omega = 0.5$ and a finite rise and fall edge of the laser field for practical consideration, we have simulated the gate fidelity with realizable polarization purity, shown in Fig. 6. The smallest gate fidelity in Fig. 6 is 0.99405 with $(\xi_0, \xi) = (0.01, 10)$. \mathcal{F} decreases slowly when ξ increases, but it is marginal. Fortunately, $1 - \mathcal{F}$ in Fig. 6 is smaller than 5.8×10^{-5} for an experimentally accessible polarization impurity, $\xi_0 \leq 10^{-4}$ [77]. These indicate that the gate can have high fidelity with affordable laser-polarization purity.

A comparison between Figs. 4 and 6 shows that using a circularly polarized laser field is more likely to yield high-fidelity gates when there is polarization impurity. This is because, for the result in Fig. 6 which is based on the laser configuration of Fig. 5, the Rydberg state that contributes most to the wrong excitation is $|r_{\downarrow}\rangle$ with a detuning that is three times larger than the detuning at $|r_{\uparrow}\rangle$, while the undesired Rydberg-excited state $|r_{-}\rangle$ is detuned from the laser that is five times larger than the detunings at the targeted Rydberg states $|r_{\uparrow}\rangle$ and $|r_{\downarrow}\rangle$. In comparison, there are two undesired Rydberg-excited states $|r_{\pm}\rangle$ with a detuning that is three times the detuning at the two targeted Rydberg states in Fig. 3, which indicates a larger probability of wrong Rydberg excitation. However, laser fields of circular polarization may be challenging to prepare and may result in lower laser power which can compromise the gate speed. Therefore, it depends on laboratory resources regarding which type of laser polarization should be used for the gate.

VI. GATES WITH FINITE RYDBERG INTERACTIONS

The gate can still attain a high fidelity when V is both finite and fluctuating. When V is finite, as shown in Eqs. (B1)–(B3) in Appendix B with a linearly polarized field, $|\alpha\beta\rangle$ can be excited to two-atom Rydberg states, leading to extra phase accumulations; this is similar for gates with a σ^+ -polarized laser field. Because the extra phase can partially arise from

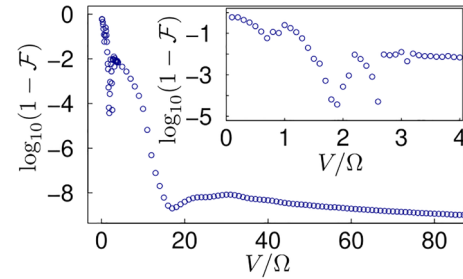


FIG. 7. Numerical gate error due to the finiteness of Rydberg interaction V . Shown is the common logarithm of infidelity of the gate as a function of V/Ω with a corresponding optimal pulse. Here, we did not start numerical optimization from the random initial phase of $\Omega(t)$, but each data point here with a certain V was found by optimizing the phase of $\Omega(t)$ obtained with infinite V , i.e., by optimizing the phase profile shown in Fig. 12(a). Inset: The zoom-in around $V/\Omega = 2$ where relatively high-fidelity gates can be realized due to the antiblockade effect.

the dynamical phase accumulation $\sim V t_{2\text{Ryd}}$ [41], with $t_{2\text{Ryd}}$ the time for the two-qubit state to be in the two-atom Rydberg state, there will be gate error due to the fluctuation of V . This means that when V does not fluctuate, there will be a possibility to realize accurate gates with $V \sim \Omega$ [37,40], but it also means that the gate fidelity can be small when V fluctuates since different V not only directly results in different dynamical phases, but also leads to different probabilities of two-atom Rydberg excitation so that $t_{2\text{Ryd}}$ fluctuates. Fortunately, when $V \gg \Omega$, the two-atom Rydberg state is barely populated due to the Rydberg blockade mechanism [50,58] so that the gate error due to the fluctuating V is small thanks to a negligible $t_{2\text{Ryd}}$.

As a common feature of optimal-control-based Rydberg gates [38,59–70], near-unit fidelity is theoretically possible when V is finite and fixed. To examine this, we take, as an example, the implementation with a σ^+ -polarized laser field. Shown in Fig. 7 is the common logarithm of infidelity of the gate as a function of V/Ω with optimized phases of $\Omega(t)$. Figure 7 shows that the gate can have a high fidelity $\mathcal{F} = 1 - 3.7 \times 10^{-5}$ when $V/\Omega = 1.9$. The high-fidelity gates around $V/\Omega = 2$ highlighted in the inset of Fig. 7 are due to the antiblockade effect [58], i.e., accurate CZ-like gates can be realized by exploring the relation between detuning and amplitude of the laser field, Rydberg interaction, and pulse duration, as studied in, e.g., Refs. [37,40,80]. Besides being useful in quantum logic gates, Rydberg antiblockade is also useful for generating a Greenberger-Horne-Zeilinger (GHZ) state, as explored in Ref. [81]. The position fluctuation of the qubits can cause fluctuation of V , which can lead to extra errors in the gate. To characterize the gate performance with fluctuating V , we choose, as an example, $V = 50\Omega$, where the pulse profile and state dynamics of typical input states of the gate are shown in Fig. 8 when V is fixed at 50Ω . The condition $V = 50\Omega$ should be experimentally feasible by placing two atoms near enough, as in Ref. [5] where a large interaction with $V \approx 98\Omega$ was used in a high-fidelity entangling gate, and $V/2\pi$ over 1 GHz was used in experimental CZ gates [16]. The gate fidelity in Fig. 8 is relatively large, with $\log_{10}(1 - \mathcal{F}) = -8.56$, so that we can treat the gate map of the case in

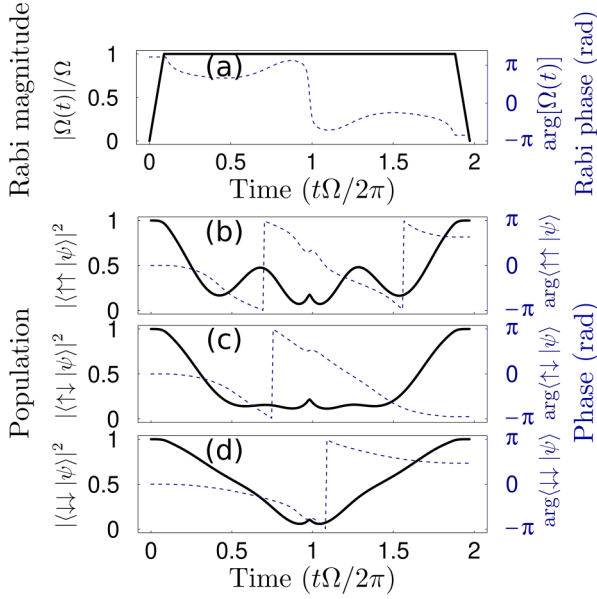


FIG. 8. State dynamics for the CZ-like gate with a finite Rydberg interaction $V = 50\Omega$, $\frac{\Delta_Z}{\Omega} = 0.5$, and σ^+ -polarized laser field, where the laser is tuned at the middle of the gap between $|r_+$ and $|r_+$. (a)–(d) show similar quantities as in Fig. 2. The final population of the ground-state wave functions in (b)–(d) is 1, and their phases are $\phi_{\uparrow\uparrow} = 1.990577$, $\phi_{\uparrow\downarrow} = -2.983394$, and $\phi_{\downarrow\downarrow} = 1.467505$, respectively. As in Fig. 2, here the gate duration is 10% longer than $2\pi N/\Omega$ where $N = 1.8$, for we have added a rise and fall edge of $\Omega(t)$, each of duration $\pi N/(10\Omega)$. We note that the phase profile in (a) here is quite close to that in Fig. 12(a), where $V/\Omega = \infty$ is assumed.

Fig. 8 as the target, i.e., $U = \text{diag}\{e^{i\phi_{\uparrow\uparrow}}, e^{i\phi_{\uparrow\downarrow}}, e^{i\phi_{\downarrow\uparrow}}, e^{i\phi_{\downarrow\downarrow}}\}$ with $\phi_{\uparrow\uparrow}$, $\phi_{\uparrow\downarrow}$, and $\phi_{\downarrow\downarrow}$ given in the caption of Fig. 8, and characterize the gate map $\mathcal{U} = \text{diag}\{ae^{i\phi'_{\uparrow\uparrow}}, be^{i\phi'_{\uparrow\downarrow}}, be^{i\phi'_{\downarrow\uparrow}}, ce^{i\phi'_{\downarrow\downarrow}}\}$ realized with a fluctuating V by the fidelity in Eq. (2). We consider the average,

$$\bar{\mathcal{F}} = \int \mathcal{F}(V)dV / \int dV, \quad (3)$$

where the integration is over $V \in 50\Omega[1 - \epsilon, 1 + \epsilon]$. Here, we use a uniform distribution of V in the fluctuating region, for in the numerics it can lead to a larger gate error compared to a Gaussian distribution so that we can estimate a lower bound for the gate fidelity. The results with $\epsilon \in [0, 0.4]$ are given in Fig. 9, which shows that the gate error is smaller than 10^{-4} (10^{-5}) when $\epsilon < 0.22$ (0.023). When we consider strong V , it usually means that it is of the dipole-dipole character, namely, it is nearer to the scaling $V \propto L^{-3}$ [58,75], with L the atomic separation, and therefore $\epsilon < 0.22$ (0.023) is satisfied when the fluctuation of L is within 7% (0.8%). With the feasibility to cool atoms to the motional ground state in optical traps which can significantly suppress the position fluctuation of the qubits [5], the relatively slow increase of gate error when ϵ increases as in Fig. 9 means that high-fidelity nuclear-spin gates are realizable.

VII. DISCUSSION AND CONCLUSION

We have studied a fast CZ-like gate with nuclear spins in a weak magnetic field by taking ^{171}Yb as an example, for

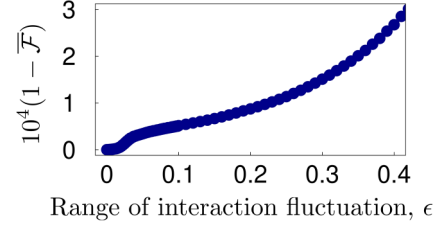


FIG. 9. Gate error from the fluctuation of V in the nuclear-spin gate (scaled by 10^4) of Eq. (3) averaged by uniformly varying the Rydberg interaction V in $50\Omega[1 - \epsilon, 1 + \epsilon]$. Each V results in a gate map \mathcal{U} different from the desired gate map, $\text{diag}\{e^{i\phi_{\uparrow\uparrow}}, e^{i\phi_{\uparrow\downarrow}}, e^{i\phi_{\downarrow\uparrow}}, e^{i\phi_{\downarrow\downarrow}}\}$, where $\phi_{\uparrow\uparrow}$, $\phi_{\uparrow\downarrow}$, and $\phi_{\downarrow\downarrow}$ are given in the caption of Fig. 8. Note that one pulse is used for the simulation here, i.e., the pulse that yields a high-fidelity gate when the interaction is exactly 50Ω .

it has the simplest nuclear spin, $I = 1/2$, which allows relatively easier manipulation in experiments [82–84]. Besides, the clock state of ^{171}Yb possessing only two nuclear-spin Zeeman substates results in that no other nuclear-spin states exist for the population to leak to [85], as shown in Fig. 3. For atoms with larger I , the theory is applicable by strong Stark shifts to shift away nearby nuclear-spin Zeeman substates as in [86] so as to suppress population leakage.

In summary, a global laser pulse with a smooth modulation of phase can induce a CZ-like gate between two atoms in their nuclear-spin qubit states when $\Delta_Z < \Omega$, where Δ_Z is the Zeeman-splitting-dominated frequency difference for the clock-Rydberg transitions of the two nuclear-spin qubit states and Ω is the maximal Rabi frequency. The minimal Δ_Z is about 0.6Ω (0.45Ω) for realizing such a gate via linearly (circularly) polarized laser fields where the gate duration is about $2.2\pi/\Delta_Z$ ($1.8\pi/\Delta_Z$), which sets the speed limit for the gate in an anticipated practically useful quantum computer based on large-scale nuclear-spin memories under a weak B field. The gate can attain a high fidelity with lasers of experimentally affordable polarization purity [77–79] and with finite and fluctuating Rydberg interactions.

ACKNOWLEDGMENTS

The research leading to the results here has received funding from the National Natural Science Foundation of China under Grants No. 12074300 and No. 11805146, the Innovation Program for Quantum Science and Technology under Grant No. 2021ZD0302100, and the Natural Science Basic Research plan in Shaanxi Province of China under Grant No. 2020JQ-287. We acknowledge the Beijing Super Cloud Center for providing HPC resources that have contributed to the research results reported within this article.

APPENDIX A: MAGNITUDES OF MAGNETIC FIELDS IN EXPERIMENTS AND MAGNETIC SENSITIVITY OF ATOMIC QUBITS

The gate in this article is of intimate relevance to the recent advancement of Rydberg-mediated gates. A B field that is weak, typically smaller than 10 G as in [5], is prerequisite for high-fidelity Rydberg-mediated entanglement because weaker

B fields have smaller fluctuation [74]. The energy of the Rydberg atom is sensitive to the magnetic field, and a fluctuation as small as 0.025 G can add an extra dephasing rate over $2\pi \times 12$ MHz to the Rydberg state [87]. In experiments of Rydberg-mediated entanglement, the magnitude of the magnetic field was 3.7 [20,21], 9 [19], 1.5 [22,25], 4.8 [23], 3 [24], 7.5 [26], 6 [28], 4.6 [30], 7 [32], 8.5 [5,17,27], and 16 G [16], with hyperfine qubits of alkali-metal atoms (the value of the B field was not explicitly indicated in some Refs. [29,31]), and 4.11 [39] and 5 G [15] for nuclear-spin qubits of ^{171}Yb . Exceptions such as 71 [14,35] or 55 [74] G used for entangling nuclear-spin-free ^{88}Sr atoms exist, but note that the qubits in [14,35,74] have qubit frequency of hundreds of THz, which is 5 (11) orders of magnitude larger than that of a hyperfine (nuclear-spin) qubit. Even in [14,35,74], a tenfold reduction of the B field was applied when Rydberg excitation was involved so as to reduce the field fluctuation. These point to the likeliness that the fast nuclear-spin gate with only one pulse shown in this article can be useful for realizing quantum devices based on nuclear-spin memories which have several prominent strengths [88].

The results in Ref. [89] indicated that the temporal fluctuation of the magnetic field can be suppressed nearly completely, and therefore only the spatial fluctuation of the magnetic field or the freely flying atoms experiencing different fields matters. In experiments with alkali-metal atoms [5,16,17,19–29,31,32], the spatial change of magnetic field Bz in a large-scale qubit array consisting of millions of atomic qubits can result in a spatial change of frequency separation of the two-qubit states that is large compared to the Rabi frequency of single-qubit Raman transitions, which was lower [5] or much lower [12,13] than $2\pi \times 1$ MHz in high-fidelity implementations. Encoding the qubit states by the two $m_F = 0$ states [5,11] of two hyperfine levels of the ground state of an alkali-metal atom incurs smaller magnetic fluctuation, but there is a field-dependent term, $\sim(\mu_B B)^2/(2\hbar E_{\text{hfs}})$ [76], in the frequency separation of the two qubits where μ_B , \hbar , and E_{hfs} are the Bohr magneton, reduced Planck constant, and hyperfine splitting, respectively. This term brought no trouble in the published experiments, but cannot be ignored in an anticipated large-scale array with practically useful millions of qubits [33] because the spatial extent of the qubit array can be quite large, especially due to the fact that most qubit arrays are in a two-dimensional space [7–9].

APPENDIX B: NUMERICAL OPTIMIZATION METHOD

We detail the numerical optimization method used in this article. Because the method used here is similar to that in Ref. [38], and also because the CZ-gate model of Ref. [38] is simpler, we outline the numerical optimization for the CZ gate in Ref. [38]. By showing the details, we hope that readers can easily write a code to cope with similar gate protocols and employ it for further study.

The time-optimal CZ gate in Ref. [38] based on qubits encoded in the hyperfine ground states of alkali-metal atoms can be numerically studied as follows. For the input states $\{|00\rangle, |01\rangle, |10\rangle, |11\rangle\}$, the ground-Rydberg excitation $|1\rangle \leftrightarrow |r\rangle$ with a Rabi frequency Ω means that $|00\rangle$ stays intact in

the rotating frame, while $|01\rangle$ and $|10\rangle$ experience similar time dynamics, so that we can study the time dynamics for the input states $|01\rangle$ and $|11\rangle$ for realizing the CZ-like gate. For $|01\rangle$, the Hamiltonian is $\hat{H}_{01} = \Omega(t)|0r\rangle\langle 01|/2 + \text{H.c.}$; for $|11\rangle$, the Hamiltonian is $\hat{H}_{11} = \Omega(t)\frac{|1r\rangle+|r1\rangle}{\sqrt{2}}(|11\rangle/\sqrt{2} + \text{H.c.})$. In the numerical optimization, we consider the Hamiltonian $\hat{H}_{\text{alkali}} = \hat{H}_{01} + \hat{H}_{11}$. This Hamiltonian will be used to evaluate the time-evolution operator \hat{U} where the off-diagonal matrix elements give information on the input-output matrix of the CZ-like gate. At the end of the gate pulse, the input states $|01\rangle$ and $|11\rangle$ are expected to become $e^{i\phi_{01}}|01\rangle$ and $e^{i\phi_{11}}|11\rangle$, where ϕ_{01} and ϕ_{11} are to be numerically located so as to yield a CZ-like gate.

With the Hamiltonian at hand, the optimization is straightforward: (1) Set up the gate duration T_{gate} in units of $2\pi/\Omega$, where Ω is the maximal value of $\Omega(t)$; divide the gate duration into Υ equal intervals with index $i = 0, 1, \dots, \Upsilon - 1$, where Υ is a large integer; set up the value of $\Omega(t)$ at each time interval (or, equivalently, time step) according to the specific laboratory requirement. For the time-optimal CZ gate in Ref. [38], $\Omega(t) = \Omega$. (2) Use random numbers as input phase φ_i for the phase of $\Omega(t)$ at each time step i . (3) Use random numbers as input values of ϕ_{01} and ϕ_{11} . (4) Set up a target for the optimization, such as the gate fidelity \mathcal{F} being larger than a certain value. (5) Tabulate the time-evolution operator $\hat{U}(i \rightarrow i+1)$ for each i , its Hermitian conjugate, and its derivative $\hat{U}'(i \rightarrow i+1)$ with respect to the phase, where $\hat{U}(i \rightarrow i+1)$ can be calculated following Ref. [48] and the derivative of $\hat{U}(i \rightarrow i+1)$ can be calculated following Ref. [49]. With these operators, the input-output matrix of the gate can be extracted using $\hat{U}(0 \rightarrow \Upsilon - 1) \equiv \prod_{i=0}^{\Upsilon-2} \hat{U}(i \rightarrow i+1)$. (6) Use a similar way as Eq. (13) of Ref. [48] to update φ_i at each time step, where “similar” as Eq. (13) of Ref. [48] emphasizes that in Ref. [48], the amplitude of the Hamiltonian is updated, but here we update the phase of the Rabi frequency. The small time step, i.e., ϵ in Eq. (13) of Ref. [48], can be set as, e.g., 0.01. This step is as follows in the numerical realization: Calculate the derivative of \mathcal{F} with respect to φ_i by using appropriate off-diagonal matrix elements in $\hat{U}(0 \rightarrow i)\hat{U}'(i \rightarrow i+1)\hat{U}(i+1 \rightarrow \Upsilon - 1)$, where the derivative plays the role of the derivative of Eq. (13) of Ref. [48]. In experiments, there can be rise and fall edges in the laser field. In Fig. 2, the phase of the laser field is fixed at the rise and fall edges; to cope with this, we can initially set the phase equal at the rise and fall edges, and update the phase at the rise steps together, and similarly at the fall time steps, so as to get a pulse profile as in Fig. 2(a). (7) After all the phases φ_i are updated, use a similar method as in step (6) to update ϕ_{01} and ϕ_{11} . (8) Check if the target has reached a value of desire or if the number of iteration has been reached. Typically, we can set $\mathcal{F} \geq 1 - 10^{-7}$ and a very large iteration number as a threshold to stop. When the search has finished without reaching the desired \mathcal{F} , it possibly means that the used value for T_{gate} is too small. Alternatively, one can use the above steps for different T_{gate} to calculate Figs. 1(b) and 1(c) of Ref. [38]. By using the above steps, less than one hour’s search on an i7 computer yielded a phase profile shown in Fig. 10(a) with $\mathcal{F} > 1 - 10^{-8}$, where the population and phase dynamics for the input states $|01\rangle$ and $|11\rangle$ are shown in Figs. 10(b) and 10(c), respectively. In experimental

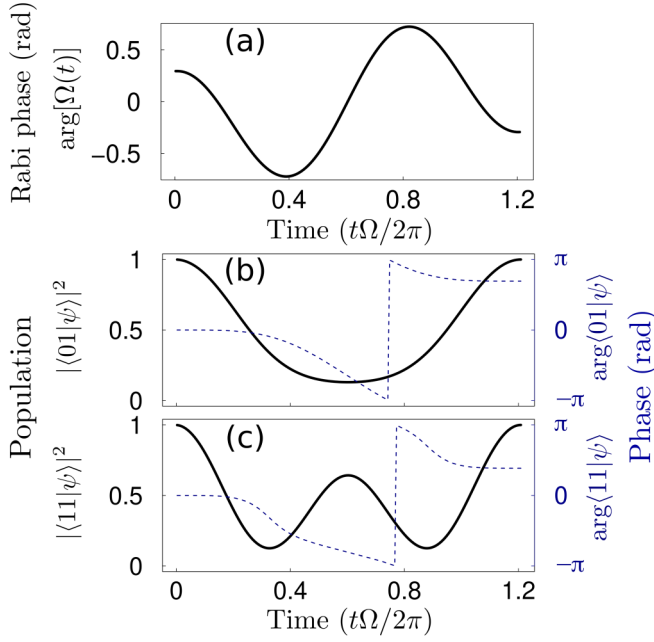


FIG. 10. State dynamics for the time-optimal CZ-like gate proposed in Ref. [38], where the qubit is encoded in, e.g., two hyperfine ground states $|0\rangle$ and $|1\rangle$, and $|1\rangle$ is excited to a Rydberg state with a Rabi frequency $\Omega(t)$ which has a constant amplitude, but a time-dependent phase. The gate duration is $T_{\text{gate}} \approx 7.612/\Omega$. (a) The phase of the Rydberg Rabi frequency. (b),(c) The population (solid curve) and phase (dashed curve) of the ground-state component of the wave function when the input states are $|01\rangle$ and $|11\rangle$, respectively. Rydberg-state decay and blockade leakage are ignored here. The final phases of the ground-state wave function are approximately (b) 2.177 967 and (c) 1.214 375 rad. The state dynamics for the input state $|10\rangle$ is similar to that of $|01\rangle$. The Rydberg superposition time is about $0.94\pi/\Omega$ averaged over the four input states.

implementation, it is not necessary to set the initial phase of the laser field to the value of Fig. 10(a), but we only need to change the phase so that $\arg[\Omega(t)] - \arg[\Omega(0)]$ is equal the corresponding $\arg\langle 01|\psi\rangle - \arg\langle 01|\psi\rangle$ shown in Fig. 10(a).

The optimization method used here is similar to the one presented above, except that the Hamiltonian is different and three out of the four input states accumulate phases that need to be searched. The Hamiltonian for the gate by a π -polarized laser field is as follows. For the input state $|\uparrow\uparrow\rangle$, the Hamiltonian is

$$\hat{H}_{\uparrow\uparrow} = \begin{pmatrix} V + 2\delta_+ & \frac{\Omega_{\uparrow\pi}}{2} & \frac{\Omega_{\uparrow\pi}}{2} & 0 \\ \frac{\Omega_{\uparrow\pi}^*}{2} & \delta_+ & 0 & \frac{\Omega_{\uparrow\pi}}{2} \\ \frac{\Omega_{\uparrow\pi}^*}{2} & 0 & \delta_+ & \frac{\Omega_{\uparrow\pi}}{2} \\ 0 & \frac{\Omega_{\uparrow\pi}^*}{2} & \frac{\Omega_{\uparrow\pi}^*}{2} & 0 \end{pmatrix} \quad (\text{B1})$$

in the basis of

$$\{|r_{\uparrow}r_{\uparrow}\rangle, |r_{\uparrow}\uparrow\rangle, |\uparrow r_{\uparrow}\rangle, |\uparrow\uparrow\rangle\},$$

where V is the Rydberg interaction, $\delta_{\pm} = -\Delta_{\pm}$, and $\Omega_{\uparrow\pi}$ ($\Omega_{\downarrow\pi}$) is the Rabi frequency for $|\uparrow\rangle$ ($|\downarrow\rangle$), with the subscript π indicating transitions induced by a π -polarized laser

field. For $|\downarrow\downarrow\rangle$, the Hamiltonian is

$$\hat{H}_{\downarrow\downarrow} = \begin{pmatrix} V + 2\delta_- & \frac{\Omega_{\downarrow\pi}}{2} & \frac{\Omega_{\downarrow\pi}}{2} & 0 \\ \frac{\Omega_{\downarrow\pi}^*}{2} & \delta_- & 0 & \frac{\Omega_{\downarrow\pi}}{2} \\ \frac{\Omega_{\downarrow\pi}^*}{2} & 0 & \delta_- & \frac{\Omega_{\downarrow\pi}}{2} \\ 0 & \frac{\Omega_{\downarrow\pi}^*}{2} & \frac{\Omega_{\downarrow\pi}^*}{2} & 0 \end{pmatrix} \quad (\text{B2})$$

in the basis of

$$\{|r_{\downarrow}r_{\downarrow}\rangle, |r_{\downarrow}\downarrow\rangle, |\downarrow r_{\downarrow}\rangle, |\downarrow\downarrow\rangle\}.$$

For $|\uparrow\downarrow\rangle$, the Hamiltonian is

$$\hat{H}_{\uparrow\downarrow} = \begin{pmatrix} V + \delta_+ + \delta_- & \frac{\Omega_{\downarrow\pi}}{2} & \frac{\Omega_{\uparrow\pi}}{2} & 0 \\ \frac{\Omega_{\downarrow\pi}^*}{2} & \delta_+ & 0 & \frac{\Omega_{\uparrow\pi}}{2} \\ \frac{\Omega_{\uparrow\pi}^*}{2} & 0 & \delta_- & \frac{\Omega_{\downarrow\pi}}{2} \\ 0 & \frac{\Omega_{\uparrow\pi}^*}{2} & \frac{\Omega_{\downarrow\pi}^*}{2} & 0 \end{pmatrix} \quad (\text{B3})$$

in the basis of

$$\{|r_{\uparrow}r_{\downarrow}\rangle, |r_{\uparrow}\downarrow\rangle, |\uparrow r_{\downarrow}\rangle, |\uparrow\downarrow\rangle\},$$

while for $|\downarrow\uparrow\rangle$, the Hamiltonian is similar to that in Eq. (B3). To have larger detuning so as to have less Rydberg population, we tune the laser field to a virtual level at the middle of the gap between $|r_{\uparrow}\rangle$ and $|r_{\downarrow}\rangle$ so that $\delta_+ = -\delta_- = \Delta_Z/2$. In the limit of large V , $|r_{\uparrow}r_{\uparrow}\rangle$ and $|\downarrow\downarrow\rangle$ are barely populated, so that a 2×2 matrix can be used for either Eq. (B1) or Eq. (B2) in the numerical optimization considering the many-body enhancement of the excitation. This means that in the large- V limit, a 7×7 matrix can be used in the numerical optimization, while the code leading to Fig. 10 only needs a 4×4 matrix. Due to the larger Hilbert space, the search for the phase profile is slower than that shown in Fig. 10(a). In this case, external computational resources can be helpful.

APPENDIX C: PULSES WITHOUT RISE AND FALL EDGES

Section III shows a numerical example of the gate when there are finite rise and fall edges in the strength of the laser field. The ramp of the laser field can be quite quick [5]. Therefore, in principle, the gate time can be made quite near to the value shown in Table I for a given B field. Then, it is worthy to study the state dynamics by assuming no rise and fall times in the laser field. Figure 11 shows the state dynamics for the CZ-like gate with $\frac{\Delta_Z}{\Omega} = 0.8$, $\Delta_{\downarrow} = -\Delta_{\uparrow} = \Delta_Z/2$ and an exact gate duration $2\pi N/\Omega$ when $N = 1.497$. Compared to Fig. 2, the phase of the Rabi frequency is smoother, but the state dynamics only shows a marginal difference.

APPENDIX D: HAMILTONIANS WITH LASER-POLARIZATION IMPURITY

With π -polarized laser fields, the gate would have unit fidelity when V is infinite. But shown in Fig. 3 are unwanted transitions from the undesired σ^{\pm} -polarized laser fields. As in Sec. IV, we suppose that the power ratio of the wrong polarization in the laser field is ζ_0 , and further use ζ to denote the power ratio of the σ^+ to the σ^- field. Although $\zeta_0 = 10^{-4}$ is possible [77], we keep ζ_0 as an unknown parameter and study

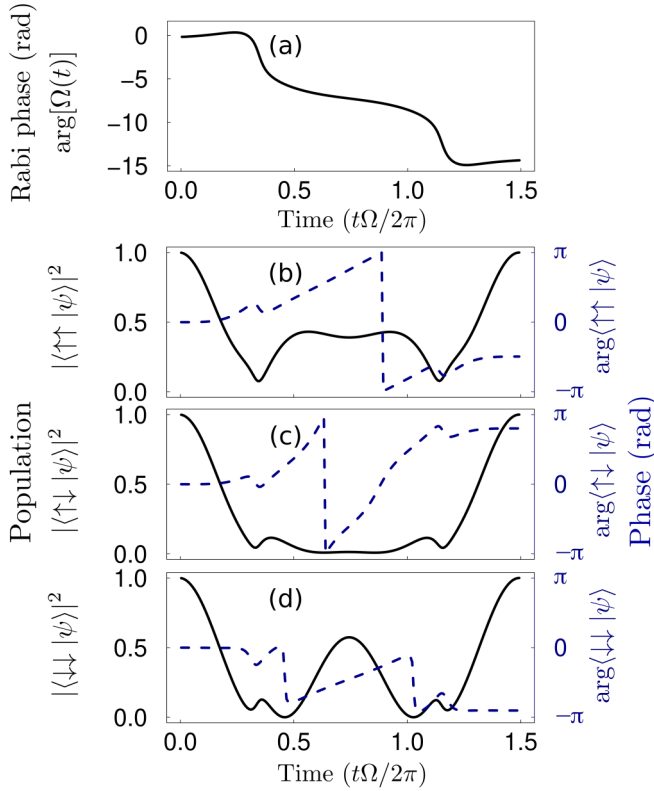


FIG. 11. State dynamics for the CZ-like gate with $\frac{\Delta_Z}{\Omega} = 0.8$, $\Delta_\downarrow = -\Delta_\uparrow = \Delta_Z/2$ and gate time $2\pi N/\Omega$ where $N = 1.497$. (a) The phase of the laser field. (b)–(d) The population (solid curve) and phase (dashed curve) of the ground-state component of the wave function when the input states are $|\uparrow\uparrow\rangle$, $|\uparrow\downarrow\rangle$, $|\downarrow\downarrow\rangle$, respectively. Rydberg-state decay and blockade leakage are ignored here. The final phases are approximately (b) -1.551073 , (c) 2.518265 , and (d) -2.837097 rad. The Rydberg superposition time is about $2\pi/\Omega$ averaged over the four input states. The counterpart to this figure, with an example of rise and fall edge, is shown in Fig. 2.

the gate fidelity with various ζ_0 . Then, the Rabi frequencies for all possible transitions are given as

$$\begin{aligned}
 |\uparrow\rangle &\rightarrow |r_\uparrow\rangle, & \text{Rabi frequency: } \Omega_{\uparrow\pi} &= \Omega(t), \\
 |\downarrow\rangle &\rightarrow |r_\downarrow\rangle, & \text{Rabi frequency: } \Omega_{\downarrow\pi} &= \Omega(t), \\
 |\uparrow\rangle &\rightarrow |r_+\rangle, & \text{Rabi frequency: } \Omega_{\uparrow+} &= \frac{\sqrt{3}}{\sqrt{2}} \sqrt{\frac{\zeta_0 \zeta}{\zeta + 1}} \Omega(t), \\
 |\downarrow\rangle &\rightarrow |r_\uparrow\rangle, & \text{Rabi frequency: } \Omega_{\downarrow+} &= \frac{1}{\sqrt{2}} \sqrt{\frac{\zeta_0 \zeta}{\zeta + 1}} \Omega(t), \\
 |\uparrow\rangle &\rightarrow |r_\downarrow\rangle, & \text{Rabi frequency: } \Omega_{\uparrow-} &= \frac{1}{\sqrt{2}} \sqrt{\frac{\zeta_0}{\zeta + 1}} \Omega(t), \\
 |\downarrow\rangle &\rightarrow |r_-\rangle, & \text{Rabi frequency: } \Omega_{\downarrow-} &= \frac{\sqrt{3}}{\sqrt{2}} \sqrt{\frac{\zeta_0}{\zeta + 1}} \Omega(t),
 \end{aligned}
 \tag{D1}$$

$$\begin{aligned}
 &\{|\uparrow r_+\rangle, |\uparrow r_\uparrow\rangle, |\uparrow r_\downarrow\rangle, |\uparrow r_-\rangle, |\downarrow r_+\rangle, |\downarrow r_\uparrow\rangle, |\downarrow r_\downarrow\rangle, |\downarrow r_-\rangle, \\
 &|r_+\uparrow\rangle, |r_\uparrow\uparrow\rangle, |r_\downarrow\uparrow\rangle, |r_-\uparrow\rangle, |r_+\downarrow\rangle, |r_\uparrow\downarrow\rangle, |r_\downarrow\downarrow\rangle, |r_-\downarrow\rangle, \\
 &|\uparrow\uparrow\rangle, |\downarrow\uparrow\rangle, |\uparrow\downarrow\rangle, |\downarrow\downarrow\rangle\},
 \end{aligned}$$

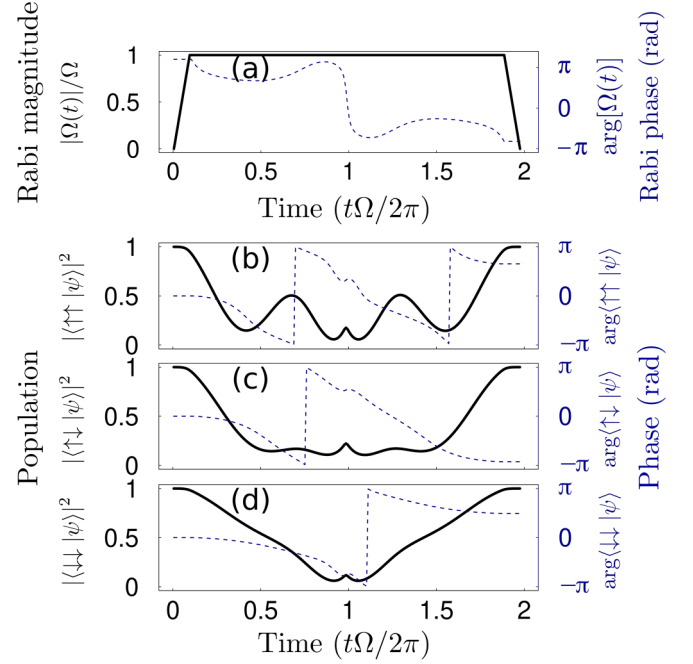


FIG. 12. State dynamics for the CZ-like gate with $\frac{\Delta_Z}{\Omega} = 0.5$ and σ^+ -polarized laser field, where the laser is tuned at the middle of the gap between $|r_+\rangle$ and $|r_\uparrow\rangle$. (a) The amplitude and phase of $\Omega(t)$. (b)–(d) The population (solid curve) and phase (dashed curve) of the ground-state component of the wave function when the input states are $|\uparrow\uparrow\rangle$, $|\uparrow\downarrow\rangle$, and $|\downarrow\downarrow\rangle$, respectively; the state dynamics for $|\downarrow\uparrow\rangle$ is similar to that of $|\uparrow\downarrow\rangle$. Rydberg-state decay and blockade leakage are ignored here. The final phases of the ground-state wave functions are (b) 2.052763 , (c) -2.910787 , and (d) 1.550441 rad. The Rydberg superposition time is about $2.2\pi/\Omega$ averaged over the four input states. As in Fig. 2, here the gate duration is 10% more than $2\pi N/\Omega$ where $N = 1.8$ for we have added a rise and fall edge of $\Omega(t)$, each of duration $\pi N/(10\Omega)$, and the rise and fall edge of the laser field has constant phases because, in real experiments, the simultaneous modulation of laser intensity and phase may be more challenging compared to the modulation of either intensity or phase. We note that the shape of the rise and fall edges can be set according to real laboratory conditions, which does not alter the numerical optimization as outlined in Appendix B, namely, an optimal phase profile of $\Omega(t)$ can be located according to specific shapes of the rise and fall edges or, more generally, according to the time dependence of the magnitude of $\Omega(t)$.

where, for brevity, we have not shown the time dependence in the Rabi frequencies. The unwanted transitions will lead to transitions between ground and single-Rydberg-excited states, so that all four computational basis states are finally connected. There are 36 basis states for the two atoms, but in the regime of strong blockade, two-atom Rydberg states are not excited, so that we consider a Hamiltonian \hat{H} with the following 20 basis states, where the texts in the brackets indicate the character of the basis states that are shown:

$$\begin{aligned}
 &[\text{control (target) atom is in the ground (Rydberg) state}] \\
 &[\text{control (target) atom is in the Rydberg (ground) state}] \\
 &(\text{both atoms are in the ground state})
 \end{aligned}$$

and $2\hat{H}$ is given by

$$\begin{pmatrix} \delta_+ & 0 & 0 & 0 & 0 & 0 & 0 & 0 & 0 & 0 & 0 & 0 & 0 & 0 & 0 & 0 & \Omega_{\uparrow+} & 0 & 0 & 0 \\ 0 & \delta_{\uparrow} & 0 & 0 & 0 & 0 & 0 & 0 & 0 & 0 & 0 & 0 & 0 & 0 & 0 & 0 & \Omega_{\uparrow\pi} & 0 & \Omega_{\downarrow+} & 0 \\ 0 & 0 & \delta_{\downarrow} & 0 & 0 & 0 & 0 & 0 & 0 & 0 & 0 & 0 & 0 & 0 & 0 & 0 & \Omega_{\uparrow-} & 0 & \Omega_{\downarrow\pi} & 0 \\ 0 & 0 & 0 & \delta_- & 0 & 0 & 0 & 0 & 0 & 0 & 0 & 0 & 0 & 0 & 0 & 0 & 0 & 0 & \Omega_{\downarrow-} & 0 \\ 0 & 0 & 0 & 0 & \delta_+ & 0 & 0 & 0 & 0 & 0 & 0 & 0 & 0 & 0 & 0 & 0 & 0 & \Omega_{\uparrow+} & 0 & 0 \\ 0 & 0 & 0 & 0 & 0 & \delta_{\uparrow} & 0 & 0 & 0 & 0 & 0 & 0 & 0 & 0 & 0 & 0 & 0 & \Omega_{\uparrow\pi} & 0 & \Omega_{\downarrow+} \\ 0 & 0 & 0 & 0 & 0 & 0 & \delta_{\downarrow} & 0 & 0 & 0 & 0 & 0 & 0 & 0 & 0 & 0 & 0 & \Omega_{\uparrow-} & 0 & \Omega_{\downarrow\pi} \\ 0 & 0 & 0 & 0 & 0 & 0 & 0 & \delta_- & 0 & 0 & 0 & 0 & 0 & 0 & 0 & 0 & 0 & 0 & 0 & \Omega_{\downarrow-} \\ 0 & 0 & 0 & 0 & 0 & 0 & 0 & 0 & \delta_+ & 0 & 0 & 0 & 0 & 0 & 0 & 0 & \Omega_{\uparrow+} & 0 & 0 & 0 \\ 0 & 0 & 0 & 0 & 0 & 0 & 0 & 0 & 0 & \delta_{\uparrow} & 0 & 0 & 0 & 0 & 0 & 0 & \Omega_{\uparrow\pi} & \Omega_{\downarrow+} & 0 & 0 \\ 0 & 0 & 0 & 0 & 0 & 0 & 0 & 0 & 0 & 0 & \delta_{\downarrow} & 0 & 0 & 0 & 0 & 0 & \Omega_{\uparrow-} & \Omega_{\downarrow\pi} & 0 & 0 \\ 0 & 0 & 0 & 0 & 0 & 0 & 0 & 0 & 0 & 0 & 0 & \delta_- & 0 & 0 & 0 & 0 & 0 & \Omega_{\downarrow-} & 0 & 0 \\ 0 & 0 & 0 & 0 & 0 & 0 & 0 & 0 & 0 & 0 & 0 & 0 & \delta_+ & 0 & 0 & 0 & 0 & 0 & \Omega_{\uparrow+} & 0 \\ 0 & 0 & 0 & 0 & 0 & 0 & 0 & 0 & 0 & 0 & 0 & 0 & 0 & \delta_{\uparrow} & 0 & 0 & 0 & 0 & \Omega_{\uparrow\pi} & \Omega_{\downarrow+} \\ 0 & 0 & 0 & 0 & 0 & 0 & 0 & 0 & 0 & 0 & 0 & 0 & 0 & 0 & \delta_{\downarrow} & 0 & 0 & 0 & \Omega_{\uparrow-} & \Omega_{\downarrow\pi} \\ 0 & 0 & 0 & 0 & 0 & 0 & 0 & 0 & 0 & 0 & 0 & 0 & 0 & 0 & 0 & \delta_- & 0 & 0 & 0 & \Omega_{\downarrow-} \\ \Omega_{\uparrow+}^* & \Omega_{\uparrow\pi}^* & \Omega_{\uparrow-}^* & 0 & 0 & 0 & 0 & 0 & \Omega_{\uparrow+}^* & \Omega_{\uparrow\pi}^* & \Omega_{\uparrow-}^* & 0 & 0 & 0 & 0 & 0 & 0 & 0 & 0 & 0 \\ 0 & 0 & 0 & 0 & \Omega_{\uparrow+}^* & \Omega_{\uparrow\pi}^* & \Omega_{\uparrow-}^* & 0 & 0 & \Omega_{\uparrow+}^* & \Omega_{\uparrow\pi}^* & \Omega_{\uparrow-}^* & 0 & 0 & 0 & 0 & 0 & 0 & 0 & 0 \\ 0 & \Omega_{\downarrow+}^* & \Omega_{\downarrow\pi}^* & \Omega_{\downarrow-}^* & 0 & 0 & 0 & 0 & 0 & 0 & 0 & 0 & \Omega_{\uparrow+}^* & \Omega_{\uparrow\pi}^* & \Omega_{\uparrow-}^* & 0 & 0 & 0 & 0 & 0 \\ 0 & 0 & 0 & 0 & 0 & \Omega_{\downarrow+}^* & \Omega_{\downarrow\pi}^* & \Omega_{\downarrow-}^* & 0 & 0 & 0 & 0 & 0 & \Omega_{\downarrow+}^* & \Omega_{\downarrow\pi}^* & \Omega_{\downarrow-}^* & 0 & 0 & 0 & 0 \end{pmatrix}, \quad (\text{D2})$$

where $\{\delta_+, \delta_{\uparrow}, \delta_{\downarrow}, \delta_-\} \equiv -2\{\Delta_{\uparrow} - \Delta_Z, \Delta_{\uparrow}, \Delta_{\downarrow} + \Delta_Z\}$. With the above Hamiltonian, we have simulated the gate fidelity with $\zeta \in [0.1, 10]$ and $\zeta_0 \in [0.0001, 0.01]$, with the results shown in Fig. 4.

We continue to examine how robust the gate is against uncertainties in laser polarization when the gate is executed by a σ^+ -polarized laser field, with an example shown in Fig. 12 when the laser is perfectly polarized. We label the power ratio between the σ^+ -, π -, and σ^- -polarized fields by $1 : \zeta_0\zeta/(1 + \zeta) : \zeta_0/(1 + \zeta)$, where ζ_0 is the intensity ratio of the wrong field to the desired field, and ζ is the ratio of the π - to the σ^- -polarized fields. Then,

$$\begin{aligned} |\uparrow\rangle &\rightarrow |r_{\uparrow}\rangle, & \text{Rabi frequency: } \Omega_{\uparrow\pi} &= \frac{\sqrt{2}}{\sqrt{3}} \sqrt{\frac{\zeta_0\zeta}{\zeta+1}} \Omega(t), \\ |\downarrow\rangle &\rightarrow |r_{\downarrow}\rangle, & \text{Rabi frequency: } \Omega_{\downarrow\pi} &= \frac{\sqrt{2}}{\sqrt{3}} \sqrt{\frac{\zeta_0\zeta}{\zeta+1}} \Omega(t), \\ |\uparrow\rangle &\rightarrow |r_+\rangle, & \text{Rabi frequency: } \Omega_{\uparrow+} &= \Omega(t), \\ |\downarrow\rangle &\rightarrow |r_{\uparrow}\rangle, & \text{Rabi frequency: } \Omega_{\downarrow+} &= \frac{1}{\sqrt{3}} \Omega(t), \\ |\uparrow\rangle &\rightarrow |r_{\downarrow}\rangle, & \text{Rabi frequency: } \Omega_{\uparrow-} &= \frac{1}{\sqrt{3}} \sqrt{\frac{\zeta_0}{\zeta+1}} \Omega(t), \\ |\downarrow\rangle &\rightarrow |r_-\rangle, & \text{Rabi frequency: } \Omega_{\downarrow-} &= \sqrt{\frac{\zeta_0}{\zeta+1}} \Omega(t), \end{aligned} \quad (\text{D3})$$

and in Eq. (D2), the diagonal terms are given via $\{\delta_+, \delta_{\uparrow}, \delta_{\downarrow}, \delta_-\} \equiv 2\{\Delta_Z, -\Delta_Z, -3\Delta_Z, -5\Delta_Z\}$ so as to have larger detunings to more effectively avoid Rydberg superposition time and undesired Rydberg excitation.

-
- [1] M. A. Nielsen and I. L. Chuang, *Quantum Computation and Quantum Information* (Cambridge University Press, Cambridge, 2000).
- [2] C. P. Williams, *Explorations in Quantum Computing*, 2nd ed., edited by D. Gries and F. B. Schneider, Texts in Computer Science (Springer-Verlag, London, 2011).
- [3] T. D. Ladd, F. Jelezko, R. Laflamme, Y. Nakamura, C. Monroe, and J. L. O'Brien, Quantum computers. *Nature (London)* **464**, 45 (2010).
- [4] Introducing IonQ Forte, Improving Quantum Performance with a Software-Configurable Dynamic Laser System, <https://investors.ionq.com/news/news-details/2022/Introducing-IonQ-Forte-Improving-Quantum-Performance-with-a-Software-Configurable-Dynamic-Laser-System/default.aspx> (unpublished).
- [5] S. J. Evered, D. Bluvstein, M. Kalinowski, S. Ebadi, T. Manovitz, H. Zhou, S. H. Li, A. A. Geim, T. T. Wang, N. Maskara, H. Levine, G. Semeghini, M. Greiner, V. Vuletic,

- and M. D. Lukin, High-fidelity parallel entangling gates on a neutral-atom quantum computer, *Nature (London)* **622**, 268 (2023).
- [6] R. Acharya *et al.*, Suppressing quantum errors by scaling a surface code logical qubit, *Nature (London)* **614**, 676 (2023).
- [7] K. N. Schymik, V. Lienhard, D. Barredo, P. Scholl, H. Williams, A. Browaeys, and T. Lahaye, Enhanced atom-by-atom assembly of arbitrary tweezer arrays, *Phys. Rev. A* **102**, 063107 (2020).
- [8] S. Ebadi, T. T. Wang, H. Levine, A. Keesling, G. Semeghini, A. Omran, D. Bluvstein, R. Samajdar, H. Pichler, W. W. Ho, S. Choi, S. Sachdev, M. Greiner, V. Vuletić, and M. D. Lukin, Quantum phases of matter on a 256-atom programmable quantum simulator, *Nature (London)* **595**, 227 (2021).
- [9] L. Pause, L. Sturm, M. Mittenbühler, S. Amann, T. Preuschoff, D. Schäffner, M. Schlosser, and G. Birkel, Supercharged two-dimensional tweezer array with more than 1000 atomic qubits, *Optica* **11**, 222 (2024).
- [10] S. Olmschenk, R. Chicireanu, K. D. Nelson, and J. V. Porto, Randomized benchmarking of atomic qubits in an optical lattice, *New J. Phys.* **12**, 113007 (2010).
- [11] T. Xia, M. Lichtman, K. Maller, A. W. Carr, M. J. Piotrowicz, L. Isenhower, and M. Saffman, Randomized benchmarking of single-qubit gates in a 2D array of neutral-atom qubits, *Phys. Rev. Lett.* **114**, 100503 (2015).
- [12] Y. Wang, A. Kumar, T.-Y. Wu, and D. S. Weiss, Single-qubit gates based on targeted phase shifts in a 3D neutral atom array, *Science* **352**, 1562 (2016).
- [13] B. Nikolov, E. Diamond-Hitchcock, J. Bass, N. L. R. Spong, and J. D. Pritchard, Randomized benchmarking using non-destructive readout in a two-dimensional atom array, *Phys. Rev. Lett.* **131**, 030602 (2023).
- [14] P. Scholl, A. L. Shaw, R. B.-S. Tsai, R. Finkelstein, J. Choi, and M. Endres, Erasure conversion in a high-fidelity Rydberg quantum simulator, *Nature (London)* **622**, 273 (2023).
- [15] S. Ma, G. Liu, P. Peng, B. Zhang, S. Jandura, A. P. Burgers, G. Pupillo, S. Puri, and J. D. Thompson, High-fidelity gates with mid-circuit erasure conversion in a metastable neutral atom qubit, *Nature (London)* **622**, 279 (2023).
- [16] T. M. Graham, Y. Song, J. Scott, C. Poole, L. Phuttitarn, K. Jooya, P. Eichler, X. Jiang, A. Marra, B. Grinkemeyer, M. Kwon, M. Ebert, J. Cherek, M. T. Lichtman, M. Gillette, J. Gilbert, D. Bowman, T. Ballance, C. Campbell, E. D. Dahl *et al.*, Multi-qubit entanglement and algorithms on a neutral-atom quantum computer, *Nature (London)* **604**, 457 (2022).
- [17] D. Bluvstein, H. Levine, G. Semeghini, T. T. Wang, S. Ebadi, M. Kalinowski, A. Keesling, N. Maskara, H. Pichler, M. Greiner, V. Vuletić, and M. D. Lukin, A quantum processor based on coherent transport of entangled atom arrays, *Nature (London)* **604**, 451 (2022).
- [18] D. Bluvstein, S. J. Evered, A. A. Geim, S. H. Li, H. Zhou, T. Manovitz, S. Ebadi, M. Cain, M. Kalinowski, D. Hangleiter, J. P. Bonilla Ataides, N. Maskara, I. Cong, X. Gao, P. Sales Rodriguez, T. Karolyshyn, G. Semeghini, M. J. Gullans, M. Greiner, V. Vuletić *et al.*, Logical quantum processor based on reconfigurable atom arrays, *Nature (London)* **626**, 58 (2024).
- [19] T. Wilk, A. Gaetan, C. Evellin, J. Wolters, Y. Miroshnychenko, P. Grangier, and A. Browaeys, Entanglement of two individual neutral atoms using Rydberg blockade, *Phys. Rev. Lett.* **104**, 010502 (2010).
- [20] L. Isenhower, E. Urban, X. L. Zhang, A. T. Gill, T. Henage, T. A. Johnson, T. G. Walker, and M. Saffman, Demonstration of a neutral atom controlled-NOT quantum gate, *Phys. Rev. Lett.* **104**, 010503 (2010).
- [21] X. L. Zhang, L. Isenhower, A. T. Gill, T. G. Walker, and M. Saffman, Deterministic entanglement of two neutral atoms via Rydberg blockade, *Phys. Rev. A* **82**, 030306(R) (2010).
- [22] K. M. Maller, M. T. Lichtman, T. Xia, Y. Sun, M. J. Piotrowicz, A. W. Carr, L. Isenhower, and M. Saffman, Rydberg-blockade controlled-NOT gate and entanglement in a two-dimensional array of neutral-atom qubits, *Phys. Rev. A* **92**, 022336 (2015).
- [23] Y.-Y. Jau, A. M. Hankin, T. Keating, I. H. Deutsch, and G. W. Biedermann, Entangling atomic spins with a Rydberg-dressed spin-flip blockade, *Nat. Phys.* **12**, 71 (2016).
- [24] Y. Zeng, P. Xu, X. He, Y. Liu, M. Liu, J. Wang, D. J. Papoular, G. V. Shlyapnikov, and M. Zhan, Entangling two individual atoms of different isotopes via Rydberg blockade, *Phys. Rev. Lett.* **119**, 160502 (2017).
- [25] H. Levine, A. Keesling, A. Omran, H. Bernien, S. Schwartz, A. S. Zibrov, M. Endres, M. Greiner, V. Vuletić, and M. D. Lukin, High-fidelity control and entanglement of Rydberg atom qubits, *Phys. Rev. Lett.* **121**, 123603 (2018).
- [26] C. J. Picken, R. Legaie, K. McDonnell, and J. D. Pritchard, Entanglement of neutral-atom qubits with long ground-Rydberg coherence times, *Quantum Sci. Technol.* **4**, 015011 (2019).
- [27] H. Levine, A. Keesling, G. Semeghini, A. Omran, T. T. Wang, S. Ebadi, H. Bernien, M. Greiner, V. Vuletić, H. Pichler, and M. D. Lukin, Parallel implementation of high-fidelity multi-qubit gates with neutral atoms, *Phys. Rev. Lett.* **123**, 170503 (2019).
- [28] T. M. Graham, M. Kwon, B. Grinkemeyer, Z. Marra, X. Jiang, M. T. Lichtman, Y. Sun, M. Ebert, and M. Saffman, Rydberg mediated entanglement in a two-dimensional neutral atom qubit array, *Phys. Rev. Lett.* **123**, 230501 (2019).
- [29] H. Jo, Y. Song, M. Kim, and J. Ahn, Rydberg atom entanglements in the weak coupling regime, *Phys. Rev. Lett.* **124**, 033603 (2020).
- [30] M. J. Martin, Y.-Y. Jau, J. Lee, A. Mitra, I. H. Deutsch, and G. W. Biedermann, A Mølmer-Sørensen gate with Rydberg-dressed atoms, [arXiv:2111.14677](https://arxiv.org/abs/2111.14677).
- [31] Z. Fu, P. Xu, Y. Sun, Y.-Y. Liu, X.-D. He, X. Li, M. Liu, R.-B. Li, J. Wang, L. Liu, and M.-S. Zhan, High-fidelity entanglement of neutral atoms via a Rydberg-mediated single-modulated-pulse controlled-PHASE gate, *Phys. Rev. A* **105**, 042430 (2022).
- [32] K. McDonnell, L. F. Keary, and J. D. Pritchard, Demonstration of a quantum gate using electromagnetically induced transparency, *Phys. Rev. Lett.* **129**, 200501 (2022).
- [33] M. Saffman, Quantum computing with neutral atoms, *Nat. Sci. Rev.* **6**, 24 (2019).
- [34] M. M. Boyd, T. Zelevinsky, A. D. Ludlow, S. Blatt, T. Zanon-Willette, S. M. Foreman, and J. Ye, Nuclear spin effects in optical lattice clocks, *Phys. Rev. A* **76**, 022510 (2007).
- [35] I. S. Madjarov, J. P. Covey, A. L. Shaw, J. Choi, A. Kale, A. Cooper, H. Pichler, V. Schkolnik, J. R. Williams, and M. Endres, High-fidelity entanglement and detection of alkaline-earth Rydberg atoms, *Nat. Phys.* **16**, 857 (2020).

- [36] A. M. Hankin, Y.-Y. Jau, L. P. Parazzoli, C. W. Chou, D. J. Armstrong, A. J. Landahl, and G. W. Biedermann, Two-atom Rydberg blockade using direct $6S$ to nP excitation, *Phys. Rev. A* **89**, 033416 (2014).
- [37] X.-F. Shi, Fast, accurate, and realizable two-qubit entangling gates by quantum interference in detuned Rabi cycles of Rydberg atoms, *Phys. Rev. Appl.* **11**, 044035 (2019).
- [38] S. Jandura and G. Pupillo, Time-optimal two- and three-qubit gates for Rydberg atoms, *Quantum* **6**, 712 (2022).
- [39] S. Ma, A. P. Burgers, G. Liu, J. Wilson, B. Zhang, and J. D. Thompson, Universal gate operations on nuclear spin qubits in an optical tweezer array of ^{171}Yb atoms, *Phys. Rev. X* **12**, 021028 (2022).
- [40] X.-F. Shi, Rydberg quantum gates free from blockade error, *Phys. Rev. Appl.* **7**, 064017 (2017).
- [41] D. Jaksch, J. I. Cirac, P. Zoller, S. L. Rolston, R. Cote, and M. D. Lukin, Fast quantum gates for neutral atoms, *Phys. Rev. Lett.* **85**, 2208 (2000).
- [42] M. D. Lukin, M. Fleischhauer, R. Cote, L. M. Duan, D. Jaksch, J. I. Cirac, and P. Zoller, Dipole blockade and quantum information processing in mesoscopic atomic ensembles, *Phys. Rev. Lett.* **87**, 037901 (2001).
- [43] X.-F. Shi, Rydberg quantum computation with nuclear spins in two-electron neutral atoms, *Front. Phys.* **16**, 52501 (2021).
- [44] X.-F. Shi, Hyperentanglement of divalent neutral atoms by Rydberg blockade, *Phys. Rev. A* **104**, 042422 (2021).
- [45] N. Chen, L. Li, W. Huie, M. Zhao, I. Vetter, C. H. Greene, and J. P. Covey, Analyzing the Rydberg-based optical-metastable-ground architecture for ^{171}Yb nuclear spins, *Phys. Rev. A* **105**, 052438 (2022).
- [46] X.-F. Shi, Fast nuclear-spin gates and electrons-nuclei entanglement of neutral atoms in weak magnetic fields, *Front. Phys.* **19**, 22203 (2024).
- [47] L. H. Pedersen, N. M. Møller, and K. Mølmer, Fidelity of quantum operations, *Phys. Lett. A* **367**, 47 (2007).
- [48] N. Khaneja, T. Reiss, C. Kehlet, T. Schulte-Herbrüggen, and S. J. Glaser, Optimal control of coupled spin dynamics: Design of NMR pulse sequences by gradient ascent algorithms, *J. Magn. Reson.* **172**, 296 (2005).
- [49] P. de Fouquieres, S. G. Schirmer, S. J. Glaser, and I. Kuprov, Second order gradient ascent pulse engineering, *J. Magn. Reson.* **212**, 412 (2011).
- [50] M. Saffman, T. G. Walker, and K. Mølmer, Quantum information with Rydberg atoms, *Rev. Mod. Phys.* **82**, 2313 (2010).
- [51] M. Saffman, Quantum computing with atomic qubits and Rydberg interactions: Progress and challenges, *J. Phys. B* **49**, 202001 (2016).
- [52] D. S. Weiss and M. Saffman, Quantum computing with neutral atoms, *Phys. Today* **70**(7), 44 (2017).
- [53] C. S. Adams, J. D. Pritchard, and J. P. Shaffer, Rydberg atom quantum technologies, *J. Phys. B* **53**, 012002 (2020).
- [54] A. Browaeys and T. Lahaye, Many-body physics with individually controlled Rydberg atoms, *Nat. Phys.* **16**, 132 (2020).
- [55] M. Morgado and S. Whitlock, Quantum simulation and computing with Rydberg-interacting qubits, *AVS Quantum Sci.* **3**, 023501 (2021).
- [56] X. Wu, X. Liang, Y. Tian, F. Yang, C. Chen, Y. C. Liu, M. K. Tey, and L. You, A concise review of Rydberg atom based quantum computation and quantum simulation, *Chin. Phys. B* **30**, 020305 (2021).
- [57] A. M. Kaufman and K. K. Ni, Quantum science with optical tweezer arrays of ultracold atoms and molecules, *Nat. Phys.* **17**, 1324 (2021).
- [58] X.-F. Shi, Quantum logic and entanglement by neutral Rydberg atoms: Methods and fidelity, *Quantum Sci. Technol.* **7**, 023002 (2022).
- [59] M. Saffman, I. I. Beterov, A. Dalal, E. J. Paez, and B. C. Sanders, Symmetric Rydberg controlled-Z gates with adiabatic pulses control target, *Phys. Rev. A* **101**, 062309 (2020).
- [60] J.-F. Wei, F.-Q. Guo, D.-Y. Wang, Y. Jia, L.-L. Yan, M. Feng, and S.-L. Su, Fast multiqubit Rydberg geometric fan-out gates with optimal control technology, *Phys. Rev. A* **105**, 042404 (2022).
- [61] X. X. Li, X. Q. Shao, and W. Li, Single temporal-pulse-modulated parameterized controlled-phase gate for Rydberg atoms, *Phys. Rev. Appl.* **18**, 044042 (2022).
- [62] S. Jandura, J. D. Thompson, and G. Pupillo, Optimizing Rydberg gates for logical qubit performance, *PRX Quantum* **4**, 020336 (2023).
- [63] M. Mohan, R. de Keijzer, and S. Kokkelmans, Robust control and optimal Rydberg states for neutral atom two-qubit gates, *Phys. Rev. Res.* **5**, 033052 (2023).
- [64] I. R. Sola, V. S. Malinovsky, J. Ahn, S. Shin, and B. Y. Chang, Two-qubit atomic gates: spatio-temporal control of Rydberg interaction, *Nanoscale* **15**, 4325 (2023).
- [65] I. R. Sola, S. Shin, and B. Y. Chang, Finding, mapping and classifying optimal protocols for two-qubit entangling gates, *Phys. Rev. A* **108**, 032620 (2023).
- [66] R. Li, J. Qian, and W. Zhang, Proposal for practical Rydberg quantum gates using a native two-photon excitation, *Quantum Sci. Technol.* **8**, 035032 (2023).
- [67] Y. Sun, Off-resonant modulated driving gate protocols for two-photon ground-Rydberg transition and finite Rydberg blockade strength, *Opt. Express* **31**, 3114 (2023).
- [68] D. K. Mark, J. Choi, A. L. Shaw, M. Endres, and S. Choi, Benchmarking quantum simulators using ergodic quantum dynamics, *Phys. Rev. Lett.* **131**, 110601 (2023).
- [69] T. H. Chang, T. N. Wang, H.-H. Jen, and Y.-C. Chen, High-fidelity Rydberg controlled-Z gates with optimized pulses, *New J. Phys.* **25**, 123007 (2023).
- [70] S. Omanakuttan, A. Mitra, E. J. Meier, M. J. Martin, and I. H. Deutsch, Qudit entanglers using quantum optimal control, *PRX Quantum* **4**, 040333 (2023).
- [71] P. W. Shor, Polynomial-time algorithms for prime factorization and discrete logarithms on a quantum computer, *SIAM J. Comput.* **26**, 1484 (1997).
- [72] L. K. Grover, Quantum mechanics helps in searching for a needle in a haystack, *Phys. Rev. Lett.* **79**, 325 (1997).
- [73] L. K. Grover, Quantum computers can search rapidly by using almost any transformation, *Phys. Rev. Lett.* **80**, 4329 (1998).
- [74] N. Schine, A. W. Young, W. J. Eckner, M. J. Martin, and A. M. Kaufman, Long-lived Bell states in an array of optical clock qubits, *Nat. Phys.* **18**, 1067 (2022).
- [75] X.-F. Shi, Transition slow-down by Rydberg interaction of neutral atoms and a fast controlled-NOT quantum gate, *Phys. Rev. Appl.* **14**, 054058 (2020).
- [76] D. A. Steck, Quantum and atom optics, <http://steck.us/teaching> (unpublished).

- [77] M. M. Dorantes, [Fast nondestructive internal state detection of neutral atoms in optical potentials](#), Universitäts- und Landesbibliothek Bonn, Ph.D. thesis, 2016.
- [78] M. Martinez-Dorantes, W. Alt, J. Gallego, S. Ghosh, L. Ratschbacher, Y. Völzke, and D. Meschede, Fast nondestructive parallel readout of neutral atom registers in optical potentials, [Phys. Rev. Lett.](#) **119**, 180503 (2017).
- [79] M. Kwon, M. F. Ebert, T. G. Walker, and M. Saffman, Parallel low-loss measurement of multiple atomic qubits, [Phys. Rev. Lett.](#) **119**, 180504 (2017).
- [80] X.-F. Shi and Y. Lu, Quantum gates with weak van der Waals interactions of neutral Rydberg atoms, [Phys. Rev. A](#) **104**, 012615 (2021).
- [81] E. Pachniak and S. A. Malinovskaya, Creation of quantum entangled states of Rydberg atoms via chirped adiabatic passage, [Sci. Rep.](#) **11**, 12980 (2021).
- [82] W. Huie, L. Li, N. Chen, X. Hu, Z. Jia, W. K. C. Sun, and J. P. Covey, Repetitive readout and real-time control of nuclear spin qubits in ^{171}Yb atoms, [PRX Quantum](#) **4**, 030337 (2023).
- [83] M. A. Norcia, W. B. Cairncross, K. Barnes, P. Battaglino, A. Brown, M. O. Brown, K. Cassella, C.-A. Chen, R. Coxe, D. Crow, J. Epstein, C. Griger, A. M. W. Jones, H. Kim, J. M. Kindem, J. King, S. S. Kondov, K. Kotru, J. Lauigan, M. Li *et al.*, Midcircuit qubit measurement and rearrangement in a ^{171}Yb atomic array, [Phys. Rev. X](#) **13**, 041034 (2023).
- [84] J. W. Lis, A. Senoo, W. F. McGrew, F. Rönchen, A. Jenkins, and A. M. Kaufman, Midcircuit operations using the omg architecture in neutral atom arrays, [Phys. Rev. X](#) **13**, 041035 (2023).
- [85] It is possible for the population to go to the ground state via blackbody and spontaneous emission. Due to the high gate speed, such population leakage is of marginal influence to the gate fidelity.
- [86] K. Barnes, P. Battaglino, B. J. Bloom, K. Cassella, R. Coxe, N. Crisosto, J. P. King, S. S. Kondov, K. Kotru, S. C. Larsen, J. Lauigan, B. J. Lester, M. McDonald, E. Megidish, S. Narayanaswami, C. Nishiguchi, R. Notermans, L. S. Peng, A. Ryou, T.-Y. Wu *et al.*, Assembly and coherent control of a register of nuclear spin qubits, [Nat. Commun.](#) **13**, 2779 (2022).
- [87] M. Saffman, X. L. Zhang, A. T. Gill, L. Isenhower, and T. G. Walker, Rydberg state mediated quantum gates and entanglement of pairs of neutral atoms, [J. Phys.: Conf. Ser.](#) **264**, 012023 (2011).
- [88] A. J. Daley, M. M. Boyd, J. Ye, and P. Zoller, Quantum computing with alkaline-earth-metal atoms, [Phys. Rev. Lett.](#) **101**, 170504 (2008).
- [89] M. Borkowski, L. Reichsöllner, P. Thekkeppatt, V. Barbé, T. van Roon, K. van Druten, and F. Schreck, Active stabilization of kilogauss magnetic fields to the ppm level for magnetoassociation on ultranarrow Feshbach resonances, [Rev. Sci. Instrum.](#) **94**, 073202 (2023).